Electronic structure of semiconductor surface inversion layers at finite temperature. The Si(100)-SiO_2 system

S. Das Sarma
*Physik-Department, Technische Universität München, D-8046 Garching, Federal Republic of Germany and Department of Physics and Astronomy, University of Maryland, College Park, Maryland 20742**

B. Vinter
Physik-Department, Technische Universität München, D-8046 Garching, Federal Republic of Germany
(Received 26 October 1981)

The electronic structure of an n-channel inversion layer in the Si-SiO_2 metal-insulator-semiconductor system is investigated at finite temperatures for the (100) surface. The subband energies for the ground state and the low-lying excited states are calculated (i) within a Hartree self-consistent-field formulation and with exchange-correlation corrections treated perturbationally in the plasmon-pole approximation and (ii) by employing a finite-temperature version of the local density functional (LDF) technique. Many-body effects are found to be important even at room temperature. A comparison of results of the two methods shows that the LDF works quite well also at finite temperatures for the unprimed subband ladder. Our results for the unprimed subbands are in good quantitative agreement with recent experimental results. For the primed subbands our results agree only qualitatively with the experiments and the two methods give considerably different results. Finally the critical temperature for the two-valley to one-valley transition is calculated to be about 4.5 K for electron densities around 10^{11} cm^{-2}.

I. INTRODUCTION

During the last decade a number of calculations of the electronic structure on n-channel inversion layers in the Si(100)-SiO_2 metal-insulator-semiconductor (MIS) system have appeared in the literature.[1-7] Early work concentrated on low temperatures where it was shown that many-body effects contribute significantly to the subband energies.[2-4] A review of this work has been given by Ando.[8] Comparison of theoretical and experimental[9-11] results has also shown that inclusion of exchange-correlation effects in the calculation is essential for good agreement.

Recently, theoretical efforts on the calculation of the electronic structure of Si inversion layers have been extended to finite temperatures.[5-7] There is a number of reasons for this interest in the effects of temperature in this system: (i) The Fermi temperature T_F of these systems is quite low, ranging from 7 to 700 K for electron densities between 10^{11} and 10^{13} cm^{-2}, unlike bulk metals where T_F is of the order of 10^4 K. Thus a variation of the temperature from liquid helium to room temperature changes the system from a degenerate quantum system to a nondegenerate, almost classical system. (ii) At finite temperatures several subbands are thermally occupied by the electrons, making the system a truly multicomponent plasma. Since the wave functions for the different subbands are very different from each other, the screening behavior of the system is drastically affected by the temperature, giving rise to an *implicit* temperature dependence of the subband structure because of the occupancy changes in addition to the *explicit* temperature dependence described in (i). (iii) Since many-body effects are significant at low temperature, it is important to explore their relative importance with increasing temperature. Again, the low value of T_F makes such an investigation interesting and relevant, since low-temperature expansions used in metal physics are not sufficient. (iv) Actual MIS devices in technological use are operated at room temperature, and (v) recent experiments in infrared absorption spectroscopy[12-14] have shown that the subbands remain well defined so that transitions between them can be observed even up to room temperature.

Especially motivated by the latter experimental results, we have carried out a calculation of the

electronic structure of the n-channel inversion layer on the Si(100) surface for a variety of temperatures $0 \leq T \leq 300$ K and inversion-layer densities 10^{11} cm$^{-2} \leq N_s \leq 3 \times 10^{12}$ cm^{-2}. In this paper we report the results of this calculation and compare them with the experiments. In an earlier communication[7] we presented some of the results and conclusions of our work.

Compared with earlier work[5,6] on subband structure at finite temperature, our present calculation differs in several aspects. Nakamura *et al.*[6] used a static random-phase approximation (RPA) to obtain the many-body corrections to the Hartree one-electron energy values. This approximation is good only in the limit of $T \to \infty$,[15] restricting their calculation to high temperatures. At low temperature it is known[2,4] that inclusion of dynamical screening gives the most important contribution to the correlation-energy corrections. Our calculation takes account of the essential dynamical aspects of RPA, but for actual computation we have used a plasmon-pole (PP) approximation[16,17] generalized for the finite-temperature multicomponent system as in Ref. 5. The differences for the self-energies in RPA and PP are known to be small at $T=0$ in both three[16] and two dimensions,[2] and it has been shown by Kalia *et al.* and Das Sarma *et al.*[5] that the plasmon-pole approximation gives the same results as static RPA at high temperatures for Si inversion layers. Thus our calculation is essentially the random-phase approximation at finite temperature.

Compared with the calculations of Das Sarma *et al.*,[5] the major improvement is that we use as a basic set the exact numerical solution[1] of the finite-temperature Schrödinger equation in the Hartree approximation instead of variationally determined wave functions. This is important quantitatively, since the variational Hartree subband energies are inaccurate by 10–20%. Another quantitatively small correction is included in the present work by adjusting the chemical potential of the interacting system to give the correct density in a self-consistent way.

In parallel with the perturbational method we have also employed a finite-temperature generalization of the local density functional (LDF) technique[3,18] to obtain the subband energies. In this method one solves the one-electron Schrödinger-type equations derived by Kohn and Sham[19] in which the effective potential contains, in addition to the Hartree potential, an exchange-correlation potential for the inhomogeneous electron gas. It was demonstrated by Ando[3,8] that for the zero-temperature case this method gives good results for the subband energies compared with experiments, and that the method is computationally much simpler than the perturbational many-body calculation. The immediate difficulty in extending the LDF method to finite temperature is the fact that no exchange-correlation potential at finite temperature has been computed for our semi-infinite system.[20]

We circumvent this problem by simply taking the exchange-correlation potential to have the same density dependence at finite temperature as at $T=0$. Thus temperature enters only implicitly in that the occupancies and thereby the density distribution change with temperature. Such a calculation can of course only be justified *a posteriori* by comparing final results with other methods and experiments, so our reason for doing this parallel calculation is twofold. On the one hand, the LDF calculation neglects any explicit temperature dependence of the many-body effects. A comparison between it and the perturbational calculation which contains both explicit and implicit (through the change in occupancies) effects of temperature gives us information on the relative importance of those two effects. On the other hand, we use the calculation to establish the temperature range in which the LDF method can be applied quantitatively. This is of interest not only for subband calculations since the method is very easily applicable to other problems. We mention that our approximation is in principle the same as the one that has been widely used in calculating thermodynamic and other finite-temperature properties of electron-hole droplets[21] in bulk silicon and germanium and to equation-of-state calculations of solids.[22] To our knowledge, ours is the first direct comparison between a finite-temperature LDF calculation and a perturbational calculation in the same system to check the validity of the simple LDF method. We find that the method works at least up to room temperature for the unprimed subband ladder.

The plan of the present paper is the following. In Sec. II we present the theory describing the finite-temperature Hartree calculation, the self-energy calculation within the PP approximation, and the LDF calculation. Although some of the material overlaps considerably with earlier papers, especially Refs. 1, 5, and 18, we provide it for completeness. In Sec. III we present and discuss our results for subband self-energies, subband ener-

gies, and subband occupancies. We compare the results of the various approximations with each other and with the infrared absorption measurements.

For the unprimed subbands we find good agreement between the theories that include many-body effects and the experiments. For the primed subband system, which is only occupied at higher temperatures, the agreement is less convincing and the LDF results also differ considerably from the perturbational ones. Having established the applicability of the LDF method for the unprimed system, we use it to investigate the critical temperature for the predicted valley condensation[23] in the Si(100) inversion layer. We conclude in Sec. IV by discussing the approximations involved in our calculation and possible ways to improve them. We also discuss effects that we have neglected. Finally, we suggest some new experiments which would illuminate more clearly the role played by many-body effects, particularly with respect to the primed subband ladder.

II. THEORY

A. Hartree approximation

Within the effective-mass approximation[1] the Hartree envelope wave function can be written as

$$\varphi_{i\vec{k}}(\vec{r},z)=A^{-1/2}e^{i\vec{k}\cdot\vec{r}}\zeta_i(z)\ , \tag{1}$$

where $\vec{k}$ and $\vec{r}$ are two-dimensional vectors in the plane parallel to the inversion layer, A is the area, z is in the direction perpendicular to the interface, and the subband wave function $\zeta_i(z)$ is determined by a one-dimensional Schrödinger equation

$$\left[-\frac{\hbar^2}{2m_{3i}}\frac{d^2}{dz^2}+V_H(z)\right]\zeta_i(z)=E_i\zeta_i(z)\ . \tag{2}$$

In Eq. (2), m_{3i} is the relevant[1] mass for motion perpendicular to the surface. The energy of the state (1) is given by

$$E_i(\vec{k})=E_i+\hbar^2k_1^2/2m_{1i}+\hbar^2k_2^2/2m_{2i}\ , \tag{3}$$

where m_{1i} and m_{2i} are the masses for motion parallel to the surface. The Hartree potential $V_H(z)$ contains the depletion potential arising from the fixed charge N_A-N_D per unit volume from ionized acceptors and donors in the depletion layer of width z_d, and the potential due to the inversion-layer electrons themselves with charge distribution

$$n(z)=\sum_i N_i\,|\,\zeta_i(z)\,|^2\ .$$

Here the occupancy N_i of subband i at temperature T is given by

$$N_i=\left[\frac{g_{vi}m_{di}}{\pi\beta\hbar^2}\right]\times\ln\{1+\exp[-\beta(E_i-\mu]\}\ , \tag{4}$$

where $\beta=(k_BT)^{-1}$, g_{vi} is the valley degeneracy, $m_{di}=(m_{1i}m_{2i})^{1/2}$ the density-of-states mass of the ith subband, and the chemical potential μ is fixed by the constraint that

$$\sum_i N_i=N_s\ , \tag{5}$$

where N_s is the total inversion-layer density per unit area. Since the depletion-layer width is usually much larger than the inversion-layer thickness, we can take the depletion-layer potential to be a linear potential $V_d(z)=e^2N_dz/\epsilon_0\kappa_s$, where the depletion charge $N_d=(N_A-N_D)z_d$, and κ_s is the semiconductor dielectric constant. We also neglect the small temperature dependence[1] of N_d.

We solve the Schrödinger equation (2) and Poisson's equation self-consistently to get E_i, $\zeta_i(z)$, N_i, and μ for a given inversion-layer density and temperature. These quantities are used as input for the calculation of self-energies as described in Sec. II B. We have included only the five subbands 0, 1, 2, 0′, 1′, where the unprimed subbands have $m_3=m_l$ and the primed have $m_3=m_t$. For temperatures up to 200 K this gives at most an error of 2 meV compared with the values of Stern[1] who included many more subbands. In the worst case of $T=300$ K the subbands 2 and 1′ are too low, whereas the lowest three subbands agree well with those of Stern. For the energy differences E_{20} and $E_{1'0'}$ the error of 6 meV is not quite negligible. Further details of the Hartree calculation can be found in Ref. 1.

B. Many-body perturbational calculation

On the basis of the Hartree wave functions [Eq. (1)], the matrix element for the interaction of two electrons initially in subbands i and l and finally in j and m, respectively, is given by[2]

$$v_{ijlm}(\vec{q})=\frac{e^2}{2\epsilon_0\kappa_s q}f_{ijlm}(q)\ , \tag{6}$$

$$f_{ijlm}(q)=\int_0^\infty dz\int_0^\infty dz'\zeta_i^*(z)\zeta_j(z)\times\left[e^{-q|z-z'|}+\frac{\kappa_s-\kappa_i}{\kappa_s+\kappa_i}e^{-q(z+z')}\right]\times\zeta_l^*(z')\zeta_m(z')\ , \tag{7}$$

where $\vec{q}$ is the momentum transfer parallel to the interface and κ_i is the dielectric constant of the insulator. The first term in the large parentheses in Eq. (7) comes from the direct Coulomb interaction, whereas the second term arises from the interaction through the image effect at the semiconductor-insulator interface. It has been shown also by explicit calculation[2,5,6] that the form factor $f_{ijlm}(q)$ is small unless $i=j$ and $l=m$. This leads to the diagonal approximation in which we assume $v_{ijlm}\propto\delta_{ij}\delta_{lm}$.

Within RPA the dynamically screened interaction[15] $U_{ijlm}(\vec{q},i\nu_m)$ defined at discrete frequencies $i\nu_m=2m\pi i/\beta\hbar$, $m=0,\pm1,\pm2$, etc., is then also diagonal and involves only diagonal elements of the noninteracting polarizability $\Pi^0_{ij}(\vec{q},i\nu_m)$. Equations for U and Π^0 can be found in Ref. 5. The Green's function for the interacting system $G_{ij}(\vec{k},i\omega_n)$ defined at discrete frequencies $i\omega_n=(2n+1)\pi i/\beta\hbar$, $n=0,\pm1,\pm2$, etc. is determined by Dyson's equation with a self-energy $M_{il}(\vec{k},i\omega_n)$ which we approximate by

$$M_{il}(\vec{k},i\omega_n)=\delta_{il}\left[-\frac{1}{\beta\hbar}\right]\sum_{i\omega_l}e^{i\omega_l\eta}\int\frac{d^2p}{(2\pi)^2}G_{ii}(\vec{p},i\omega_l)U_{iiii}(\vec{k}-\vec{p},i\omega_n-i\omega_l)\ , \tag{8}$$

where $\eta=0+$, which is basically the random-phase approximation, but extended by having the interacting rather than the noninteracting Green's function in the integral. Dyson's equation can then be solved:

$$G_{ij}(\vec{k},i\omega_n)=\frac{\delta_{ij}}{i\omega_n-\hbar^{-1}[E_i(\vec{k})-\mu]-M_{ii}(\vec{k},i\omega_n)}\ . \tag{9}$$

The quasiparticle energies inluding exchange-correlation effects are given by the poles of the retarded Green's function obtained from Eq. (9) by analytic continuation $i\omega_n\to\omega+i\eta$. Thus quasiparticles are given by the solution of the equation (also called Dyson's equation)

$$E_i^*(\vec{k})\equiv\hbar\omega_i^*(\vec{k})+\mu=E_i(\vec{k})+M_{ii}(\vec{k},\omega_i^*(\vec{k}))\ . \tag{10}$$

In general, $M_{ii}(\vec{k},i\omega_n\to\omega+i\eta)$ will have real and imaginary parts and Eq. (10) gives both the quasiparticle energy (real part) and the lifetime (inverse of the imaginary part). Here we are interested in the electronic energy levels including many-body effects. Therefore we have neglected the imaginary part of the self-energy in Eq. (10).

Once $\mathrm{Re}M_{ii}(\vec{k},i\omega_n\to\omega+i\eta)$ has been calculated from Eq. (8), one can solve Eq. (10) by iteration to obtain the subband energies, including many-body effects. Instead of solving it exactly, we take only the first iteration in which $M_{ii}(\vec{k},\omega+i\eta)$ is evaluated at $\omega=E_i(\vec{k})-\mu$. Arguments have been suggested for[24,25] and against[26,2] this procedure, and in the context of Si inversion layers both these procedures [solving Eq. (10) (Ref. 2) and taking the first iteration only[4,5,26]] have been employed. Quantitatively the difference between the two procedures is about 5 meV for the self-energy at $T=0$ K [see Fig. 3 of Ref. 2(b)], but we have not tried to estimate the difference at higher temperatures. We shall return to this point in Sec. IV. Finally putting $\vec{k}=0$ in Eq. (10) we get the subband bottom energy including exchange and correlation:

$$E_i^*=E_i+\mathrm{Re}M_{ii}(k=0,E_i-\mu)\ , \tag{11}$$

where the energy argument of M_{ii} is understood to have the $i\eta$ in it.

In the actual computation of Eq. (8) we make one further approximation: we use the plasmon-pole (PP) approximation for the screened interaction. The spirit of this approximation is rather simple.[16,17] Instead of considering the full dynamically screened interaction $U_{ijll}(\vec{q},\omega)$, one takes its spectral function [or $\mathrm{Im}U(\vec{k},\omega+i\eta)$] to be a δ function in frequency with suitable strength. The strength and frequency are fixed by the f-sum rule and a Kramers-Kronig dispersion relation. This method can be generalized to a multicomponent plasma,[5,26] and for details we refer the reader to those papers. With this approximation the frequency sum in Eq. (8) is easily done, and one is left with a two-dimensional wave-vector integration which becomes a one-dimensional integral over $q=|\vec{q}|$ if one is interested in the bottoms of the subbands ($\vec{k}=0$). We have found $M_{ii}(\vec{k},\omega+i\eta)$ to

have negligible k dependence up to about 2 k_F (where k_F is the Fermi wave vector at $T=0$) for the subbands (0, 1, 2, 0′, 1′) we have investigated. Thus the self-energy correction produces essentially only a rigid shift of the subbands, preserving the parabolic energy dispersion of Eq. (3), but with modified subband bottom energies E_i^* defined by Eq. (11).

In calculating the self-energy according to Eq. (8) a problem arises in that the self-energy M_{ii} depends on the Green's function G_{ii} which again depends on M_{ii}. We therefore calculate M_{ii} iteratively in an approximately self-consistent way and at the same time adjust μ so that the inversion-layer density in the interacting system is the one given as input. We find, however, that the final results for the self-energy are not quantitatively much different (less than 10%) from those of conventional RPA in which one has G^0 instead of G in Eq. (8).

C. Local density functional calculation

As explained in the Introduction, we use a finite-temperature generalization of the LDF method which has earlier been employed successfully to the subband structure at zero temperature.[3,18]

We consider the one-electron equations derived by Kohn and Sham[19] for the inversion-layer problem which formally are the same as the Schrödinger equation (2) but with an effective potential $V_{\rm eff}(z)$ replacing the Hartree potential:

$$\left[-\frac{\hbar^2}{3m_{3i}}\frac{d^2}{dz^2}+V_{\rm eff}(z)\right]\phi_i(z)=\epsilon_i\phi_i(z)\ . \qquad (12)$$

The effective potential contains in addition to the Hartree potential a local exchange-correlation potential $V_{\rm xc}$. By analogy with the spin-density functional formalism[27] this potential is different for primed and unprimed valleys,[18] and it depends only on the volume density of electrons in the unprimed subbands and in the primed subbands, and furthermore has an explicit dependence on z which describes approximately the image effect in the electron-electron interaction.[3] Once the functional form of $V_{\rm xc}$ is known, we solve self-consistently Eq. (12), where the electron density determines the effective potential and is itself determined by the wave functions $\phi_i(z)$ through Eqs. (2)—(5) in which $\phi_i(z)$ ϵ_i replace $\zeta_i(z)$ and E_i, respectively; temperature enters only through Eq. (4). Further details can be found in Refs. 3 and 18. The energies ϵ_i and the wave functions ϕ_i are identified as subband bottom energies and envelope wave functions including exchange-correlation effects. The exchange-correlation potential used here is the same as the one used in Ref. 18, but in contrast to that calculation we take a valley degeneracy of four in the primed subbands in the present calculation.

III. RESULTS AND DISCUSSION

We have calculated self-energies, quasiparticle energies, and subband occupancies at a variety of temperatures and inversion-layer concentrations. The set of parameters used in our calculation is listed in Table I. Unless otherwise stated all our calculations are for depletion density $N_d=6\times10^{10}$ cm^{-2} to correspond to the experimental values in Refs. 13 and 14.

TABLE I. Parameters used in the calculations.

Valleys		Unprimed	Primed
Degeneracy	g_v	2	4
Perpendicular mass	m_3	$0.916m_e$	$0.1905m_e$
Parallel masses	m_1	$0.1905m_e$	$0.1905m_e$
	m_2	$0.1905m_e$	$0.916m_e$
Optical mass[a]	$m_{\rm op}$	$0.1905m_e$	$0.315m_e$
Density of states mass[b]	m_d	$0.1905m_e$	$0.417m_e$
Dielectric constants	κ_s	11.7	
	κ_i	3.9	
Depletion-layer density[c]	N_d	6×10^{10} cm^{-2}	

[a] $m_{\rm op}=m_1m_2/(m_1+m_2)$.
[b] $m_d=(m_1m_2)^{1/2}$.
[c] Corresponding to Ref. 13. For Fig. 10, $N_d=10^{11}$ cm^{-2}.

A. Self-energy

In Figs. 1 and 2 we present results for the self-energies at subband bottoms. As we have indicated before, the calculated self-energies have little dependence on wave vector. The self-energy is usually discussed in terms of an exchange part and a correlation part:

$$M_{ii}(\vec{k},i\omega_n)=M_{ii}^x(\vec{k})+M_{ii}^c(\vec{k},i\omega_n)\ , \tag{13}$$

where the exchange part is defined in the usual manner as

$$M_{ii}^x(\vec{k})=-\int\frac{d^2p}{(2\pi)^2}n_i(\vec{p})v_{iiii}(\vec{k}-\vec{p})\ , \tag{14}$$

and the rest is the correlation part which can be written

$$M_{ii}^c(\vec{k},i\omega_n)=-\int\frac{d^2p}{(2\pi)^2}\int_{-\infty}^{\infty}\frac{d\omega'}{2\pi}\frac{f_i(\vec{p},\omega')[n_i(\vec{k}-\vec{p})+\alpha(\omega')]}{i\omega_n-\hbar^{-1}[E_i(\vec{k}-\vec{p})-\mu]}\ . \tag{15}$$

In these equations we have introduced

$$n_i(\vec{q})=(1+\exp\{\beta[E_i(\vec{q})-\mu]\})^{-1}\ , \tag{16}$$

$$\alpha(\omega)=(e^{-\beta\omega}-1)^{-1}\ , \tag{17}$$

$$f_i(\vec{q},\omega)=-2\,\mathrm{Im}U_{iiii}(\vec{q},i\nu_m\rightarrow\omega+i\eta)\ . \tag{18}$$

In Fig. 1. we show the magnitudes of the total self-energies M_0 and M_1 for the subbands 0 and 1, respectively, together with the exchange parts E_{x0} and E_{x1} as a function of temperature for the inversion-layer concentration $N_s=1\times10^{12}$ cm^{-2}. At low T all electrons are in the ground subband 0, which therefore has a large exchange energy, whereas the subband 1 being unoccupied at low T has no exchange contribution. As temperature rises, the exchange energy in subband 0 decreases in magnitude for two reasons: Electrons are thermally excited out of subband 0, so its occupancy is reduced; this is the implicit effect. In addition there is the explicit effect that the thermal broadening of the Fermi distribution function tends to reduce the exchange term, even if the occupancy was the same. The explicit effect alone would be a function of T/T_F only, where T_F is

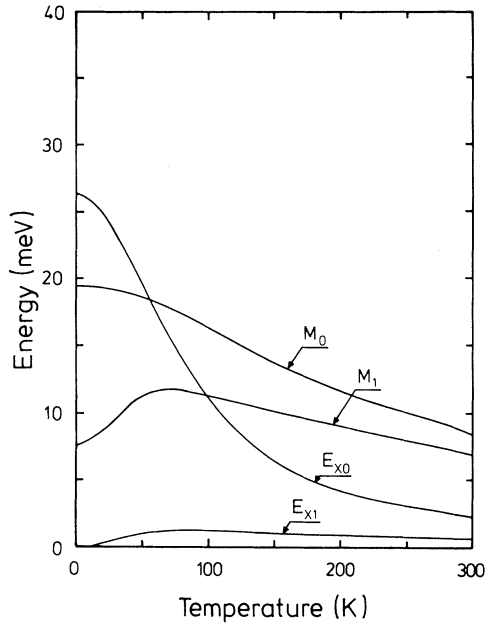

FIG. 1. Temperature dependence of the magnitudes of total self-energies M_0 and M_1 and of exchange energies E_{x0} and E_{x1} at the bottoms of subbands 0 and 1, respectively. The inversion-layer density N_s is 10^{12} cm^{-2} and the depletion-layer density N_d is 6×10^{10} cm^{-2}.

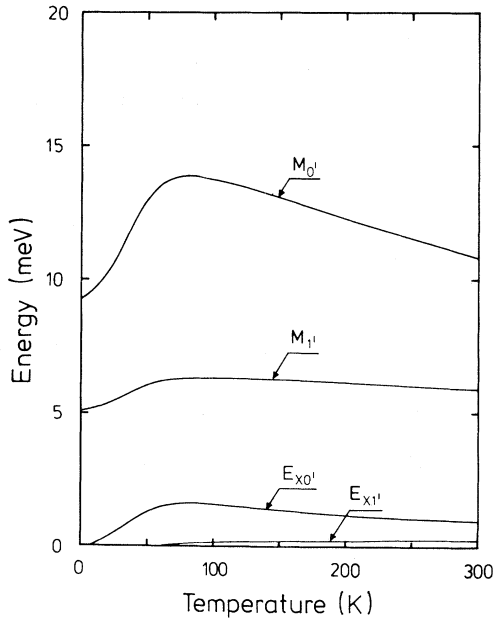

FIG. 2. Same quantities as in Fig. 1 for subbands 0′ and 1′ at same values of the densities.

the Fermi temprature $k_B T_F = E_F$ in the quantum limit, where E_F is proportional to N_s. At $N_s = 10^{12}$ cm^{-2} we have $T_F = 73$ K. On the other hand, the implicit (occupancy) effect cannot be described by a single parameter, since at finite T several subbands can be populated, so that many parameters corresponding to the subband separations enter in a complicated way. The exchange energy E_{x1} in subband 1 increases with temperature from zero to a small saturation value because of the thermal population of that subband.

The total self-energies M_0 and M_1 do not show quite such pronounced dependence on temperature, but the trend is roughly similar. Two features should be noted, however: Even at large $T \sim 300$ K, the individual self-energy corrections are quite large, ~ 10 meV. The difference $|M_0 - M_1|$, however, goes down appreciably with increasing temperature primarily because E_{x0} becomes small at high temperatures, and the correlation-energy corrections to the two subbands become similar. Thus the many-body corrections to the subband energy difference become rather small for the unprimed ladder at high temperatures. This answers the initially puzzling question,[13,14] why the Hartree calculation gives results close to the experimental values of infrared absorption at high temperatures.

In Fig. 2 we show the magnitudes of the total self-energy corrections $M_{0'}$ and $M_{1'}$ and the exchange corrections $E_{x0'}$ and $E_{x1'}$ to the lowest-lying subbands 0′ and 1′ of the primed ladder with a valley degeneracy of four. These subbands have an anisotropic mass for motion parallel to the surface. In our calculation we incorporate this anisotropy exactly in the exchange calculation. For the correlation energy we find only small differences (less than 1 meV) between using the isotropic optical and density-of-states masses for parallel motion. Thus we expect the mass anisotropy to have little effect on the self-energies.

The self-energies $M_{0'}$ and $M_{1'}$ both increase with temperature initially with $M_{0'}$ increasing appreciably. This is primarily due to the increase in the exchange contributions because the primed subbands become thermally populated rather fast with increasing temperature because of their high density of states. Above 200 K subband 0′ has a higher population than the ground subband 0. Unlike in the unprimed ladder, the self-energy corrections are quite different quantitatively also at room temperature, which explains the large observed discrepancy between the Hartree calculation and the infrared absorption measurements[13,14] for the $0' - 1'$ transition observed at high temperatures when 0′ is appreciably populated.

B. Subband energies

We now show subband energy differences in various approximations, since these are more interesting from an experimental point of view than the energy levels themselves. In Figs. 3–6 we present results for E_{10}, $E_{0'0}$, $E_{1'0'}$, and E_{20}, respectively, where $E_{ji} = E_j - E_i$, as a function of temperature from 0–300 K at a fixed inversion-layer density $N_s = 1 \times 10^{12}$ cm^{-2}. The curves are calculated results labeled *a* for Hartree, *b* for many-body perturbational with self-consistent Hartree basis, *c* for local density functional, and *d* for a many-body perturbational calculation with a variational solution to the Hartree approximation as basis. Curves *d* are included for comparison with previous work[5].

In Fig. 3 we find that the many-body perturbational (curve *b*) and the LDF calculation (curve *c*)

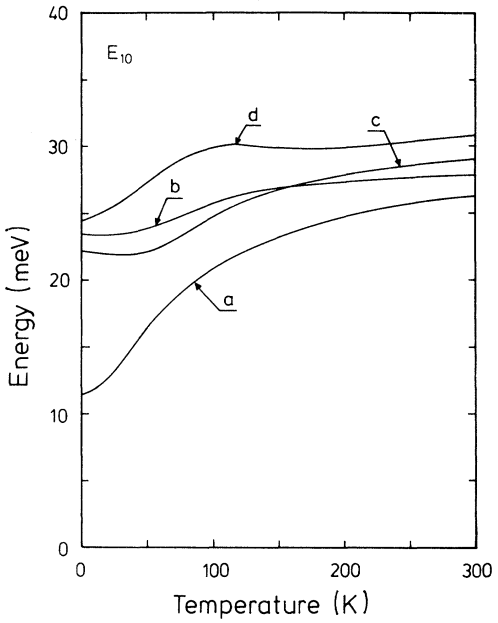

FIG. 3. Subband energy difference E_{10} as a function of temperature for the inversion-layer density $N_s = 10^{12}$ cm^{-2} and depletion-layer density $N_d = 6 \times 10^{10}$ cm^{-2} in four different approximations: *a*, Hartree self-consistent calculation; *b*, many-body perturbational calculation with Hartree basis; *c*, finite temperature local density functional calculation; *d*, many-body perturbational calculation with variational solution to Hartree approximation as basis.

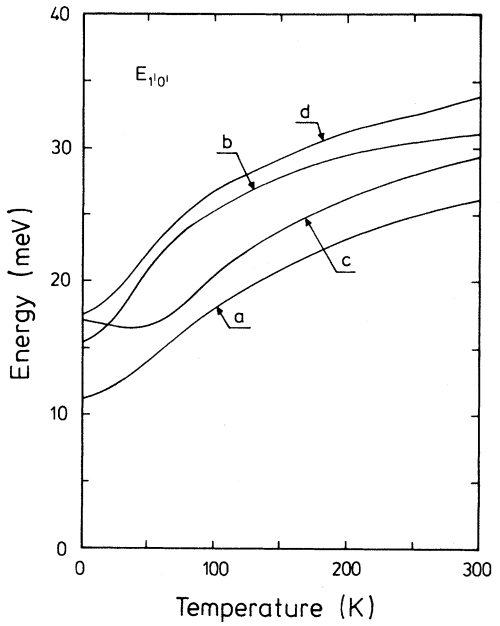

FIG. 4. Temperature dependence of subband energy difference $E_{1'0'}$ for the same parameters and with the same labeling as in Fig. 3.

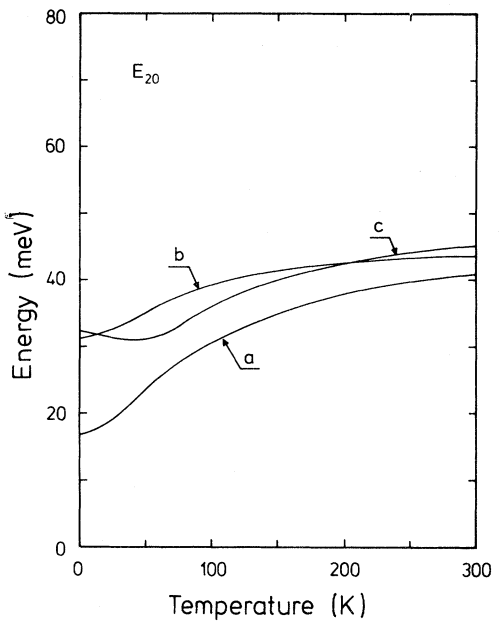

FIG. 6. Temperature dependence of subband energy difference E_{20} for the same parameters and with the same labeling as in Fig. 3.

gives similar results for E_{10} over the whole temperature range, whereas the variational basis (curve *d*) gives results considerably above those. There is a large exchange-correlation correction to E_{10} at low temperatures, as can be seen by comparing curves *b* or *c* with the Hartree result in curve *a*. However, at higher temperatures the many-body corrections to E_{10} go down in magnitude, as we have explained earlier, so that curves *a*, *b*, and *c* lie close to each other at $T=300$ K. Overall the Hartree results show much stronger temperature dependence than the results including the many-body effects. The latter remain almost temperature independent up to about 50 K and then rise slowly with T.

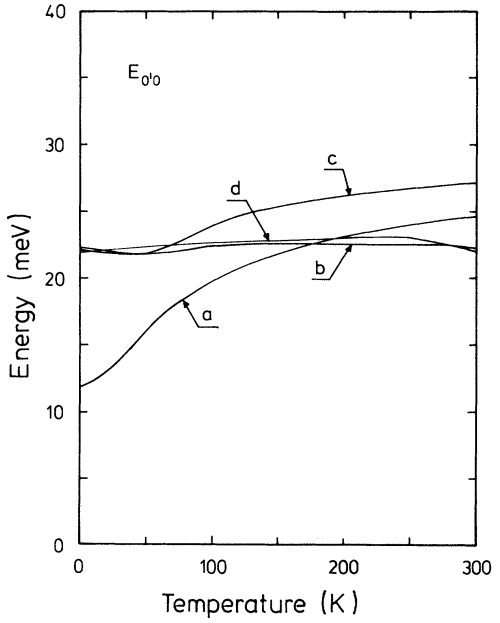

FIG. 5. Temperature dependence of subband energy difference $E_{0'0}$ for the same parameters and with the same labeling as in Fig. 3.

In Fig. 4 we show $E_{1'0'}$ as a function of temperature in the different approximations. We can see a number of qualitative differences from the results on E_{10}. $E_{1'0'}$ shows a stronger temperature dependence than E_{10}. Also, the many-body correction to $E_{1'0'}$ is rather large (compare curves *a* and *b*), even at $T=300$ K. Finally the LDF (curve *c*) and the perturbational (curve *b*) calculations do not agree well for $E_{1'0'}$, indicating that the finite-temperature generalization of the LDF technique may not be working very well for $E_{1'0'}$. In general, exchange-correlation effects contribute significantly to the subband structure of the primed ladder in the whole temperature range 0–300 K.

In Fig. 5 we depict the temperature variation of $E_{0'0}$. We see that the LDF and perturbational results agree only up to about 50 K. In Fig. 6 we have shown the temperature dependence of E_{20} which is qualitatively similar to that of E_{10} shown

in Fig. 3. The difference between Hartree and many-body results is rather large at low temperatures, going down appreciably with increasing temperature. The LDF method gives results reasonably close to the perturbational calculation, making it a meaningful procedure to use at finite temperature for the unprimed subband ladder. Because of numerical difficulties with the variational method for subband two, we have not shown results in that approximation in Fig. 6.

We now turn to the density dependence of the subband energy differences. In Figs. 7 and 8 we shown E_{10} and $E_{1'0'}$, respectively, as functions of density at $T=100$ and 300 K. We have also put the experimental points from Refs. 13 and 14 in the figures. The measurements are standard infrared absorption measurements in which the inversion-layer density is tuned by changing the gate voltage, and one looks for resonant absorption of incident radiation of a fixed frequency. It is well known that the resonance energy is not simply the subband energy separation, so strictly the comparison made in the figures is not correct. However, we argue in Sec. IV that, given our lack of safe quantitative estimates of the corrections and the problems in connection with Dyson's equation mentioned in Sec. II B, the comparison made is as good as any within the expected accuracy of our theory.

As can be seen from Fig. 7, all the approximation give reasonable agreement with experiment for $T>100$ K, with the many-body results being somewhat better. This is in sharp contrast with the zero-temperature case[2–4,8] where Hartree results give much poorer agreement and inclusion of exchange-correlation effects is essential in comparing with experiment. As we have shown earlier, the reason for the apparently good agreement between the Hartree calculation and the measurements at elevated temperatures is not the disappearance of many-body effects but a cancellation of similar self-energy corrections to both subbands 0 and 1.

For the primed subbands we have a different situation shown in Fig. 8. Exchange-correlation effects do not cancel out in $E_{1'0'}$. Thus the Hartree results (curve *a*) remain well below the many-body results (curve *b*) also at high temperatures. We also note that the LDF calculation of curve *c* gives results quite different from the perturbational ones. Finally, even though there are fewer experimental points, it is clear that the perturbational calculation

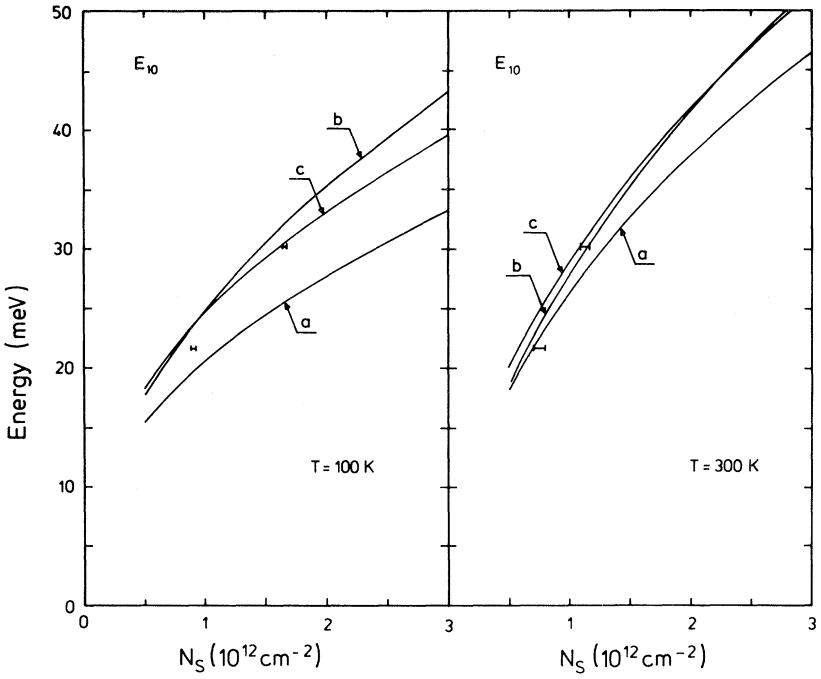

FIG. 7. Subband energy separation E_{10} as a function of inversion layer density at temperatures $T=100$ K (left) and $T=300$ K (right) in (*a*) Hartree, (*b*) perturbational, and (*c*) density functional approximations. Depletion-layer density $N_d=6\times10^{10}$ cm^{-2}. Experimental resonance energies from Ref. 13 are also shown.

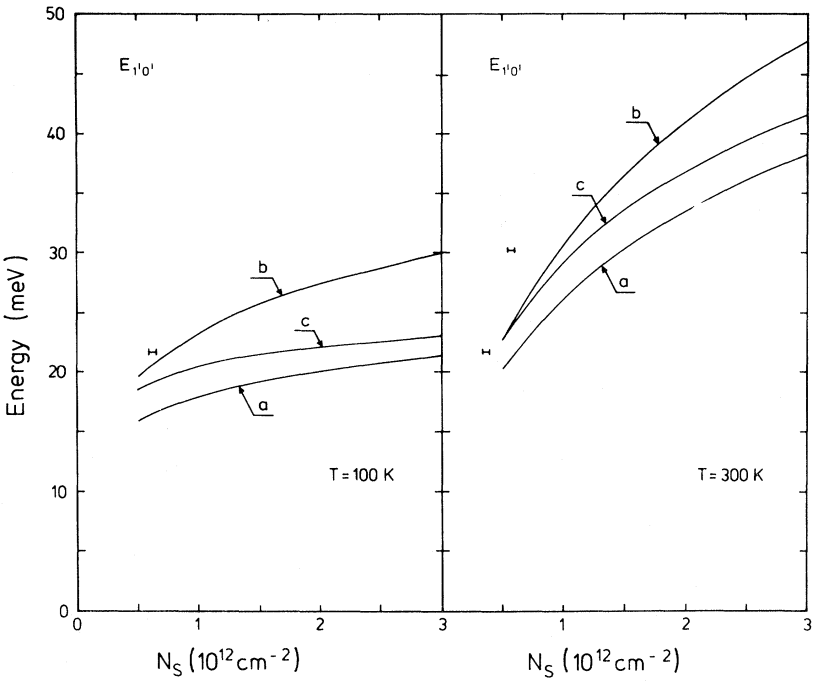

FIG. 8. Subband energy separation $E_{1'0'}$ as a function of inversion-layer density at $T=100$ K (left) and $T=300$ K (right). Parameters and labeling are the same as in Fig. 7. Experimental points from Ref. 13.

is the closest to the measured subband separations, although the agreement is decidedly poorer than for the unprimed subbands.

Two possible sources of this discrepancy can be mentioned. First, $E_{1'0'}$ depends on the occupancy of subband 0′ which in turn depends strongly on the energy separation $E_{0'0}$ which cannot be determined experimentally with the same accuracy as subband separations within the same ladder. Thus we have no good experimental check on the position of $E_{0'}$. Furthermore, it has been shown by Stern[28] that $E_{0'0}$ is rather sensitive to the boundary condition one uses at the seminconductor-insulator interface. Usually one assumes $\zeta(z)$ to vanish at the interface $z=0$, as we have done here, but if one takes into account that the potential barrier is finite and possibly not infinitely steep so that the wave functions have a short tail into the insulator, the energy separation $E_{0'0}$ is significantly reduced, whereas separations within the same ladder are not affected much. Also, the calculations beyond the simplest effective-mass approximation by Nakayama[29] show that $E_{0'0}$ depends strongly on the boundary condition at the interface although the effect is to increase $E_{0'0}$. Since the actual magnitude of these effects depends on the interface quality, it is not well known in the actual samples, which contributes to the uncertainty in comparison between experiments and our calculation. Second, the random-phase approximation may not be very good for the primed subbands. The relative importance of electron-electron interactions is usually described by the dimensionless parameter r_s, defined by

$$r_s=\frac{m_{||}e^2}{\hbar^2 4\pi\epsilon_0\bar{\kappa}\sqrt{\pi N_s}}=\frac{1}{a_0^*\sqrt{\pi N_s}}\ , \tag{19}$$

where $m_{||}$ is the mass for planar motion $\bar{\kappa}=(\kappa_s+\kappa_i)/2$, and a_0^* is the effective Bohr radius. Many-body effects are more important[15,30] at larger values of r_s whereas the kinetic energy dominates at small values of r_s. From (19) we conclude that generally the electron-electron interaction should have larger effects on the primed subbands than on the unprimed ones because of their larger $m_{||}$. Also, the higher valley degeneracy increases the importance of the many-body effects. Since RPA is a perturbational expansion in the parameter r_s, it is quite conceivable that it is not sufficient for the primed subbands.

For a better understanding of the electronic structure of the primed subbands we suggest that one should experimentally eliminate the first un-

certainty by doing the infrared absorption measurement at low temperatures under uniaxial stress such that two or all four valleys from which the primed subbands originate are lowered energetically with respect to the other valleys. Under suitable and experimentally accessible stress the subband 0′ can go well below subband 0 and become the only occupied ground subband of the system. That this can be achieved has already been demonstrated in cyclotron resonance experiments.[31] A comparison of calculations and experimental measurements of intersubband spectroscopy of $E_{1'0'}$ under such conditions would give a much clearer picture of the role of many-body effects in those subbands. We believe that the present calculations indicate that such experiments would be highly desirable.

C. Subband occupancies

In Fig. 9 we show the relative occupancies n_0 and $n_{0'}$ for subbands 0 and 0′, respectively, as functions of temperature at a fixed inversion-layer density $N_s=10^{12}$ cm^{-2}. Results of many-body perturbational (curves *b*) and LDF (curves *c*) calculations are shown. The quantity n_i is defined as $n_i=N_i/N_s$, where N_i is the actual occupancy of the ith level. We conclude that both approximations give similar results, and around 200 K subband 0′ starts having a higher population because of its higher density of states. Hartree theory gives a somewhat different trend for the subband occupancies, even though the crossover takes place in the same temperature range slightly below 200 K.

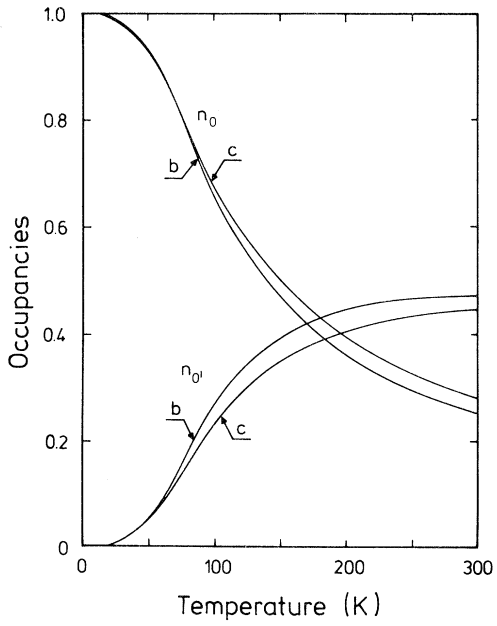

FIG. 9. Temperature dependence of relative subband occupancies n_0 and $n_{0'}$ for the inversion-layer density $N_s=10^{12}$ cm^{-2} and the depletion-layer density $N_d=6\times10^{10}$ cm^{-2} in (*b*) perturbational and (*c*) density functional approximations.

D. Valley condensation

Within the effective-mass approximation the ground-state subband 0 of the Si(100) inversion layer has a twofold valley degeneracy.[32] Normally the kinetic energy dominates, so both valleys are equally occupied. However, the exchange term tends to prefer a "valley condensation" in which only one of the two valleys is occupied by electrons, and at low densities (large r_s) the exchange term is expected to dominate, so that a transition from a two-valley to one-valley phase may become possible. This possibility was investigated at $T=0$ by Bloss *et al.*[23] who predicted a valley condensation at about $N_s\cong2\times10^{11}$ cm^{-2} for a depletion density of $N_d=1\times10^{11}$ cm^{-2}. Because of the important, experimental repercussions shown to result from this phenomenon[23] it is of interest to study the temperature dependence since temperature acts as an additional kinetic energy which above a critical temperature must "melt" the valley condensate, i.e., reestablish the double valley degeneracy.

Encouraged by the favorable agreement between the LDF method and the many-body perturbational method and experiments for the unprimed ladder, we have applied the simple extension to finite temperature of the local valley density functional technique used earlier[23] at zero temperature to this problem. In Fig. 10 we depict the critical curve for the phase transition; electrons are in the condensed (*C*) phase occupying only one valley below the curve, whereas they occupy both valleys and are in a molten (*M*) phase above the curve. As expected,[23] at zero temperature the phase transition occurs at about $N_s=2\times10^{11}$ cm^{-2}. However, at that critical density an infinitesimal temperature would melt the condensed state. The melting curve rises rather fast and we have a melting temperature of about 4.5 K for 1×10^{11} cm$^{-2}<N_s<2\times10^{11}$ cm^{-2}. Below 1×10^{11} cm^{-2} correlation starts dominating exchange, making the condensed phase less preferred so the melting temperature goes down, at least in our approximation.

Our calculation shows that the valley-condensation phenomenon would show interesting tempera-

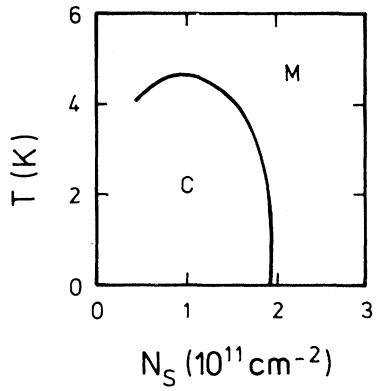

FIG. 10. Calculated temperature (T)-density (N_s) critical curve for two-valley to one-valley condensation in the ground state of the Si(100) n-channel inversion layer. Phase C is the one-valley phase and M is the two-valley phase. The depletion charge is $N_d = 10^{11}$ cm^{-2}.

ture effects, and this should be kept in mind in any experimental search for this transition. It must also be mentioned that the critical densities and temperatures occur at a very delicate balance of energies, so that the actual numbers calculated cannot be expected to be very accurate. Still, the trend in Fig. 10 should be quite correct.

IV. SUMMARY AND CONCLUSION

We have presented detailed results of theoretical calculations of the electronic structure of n-channel inversion layers in the Si(100)-SiO_2 MIS system. Corrections owing to exchange and correlation effects are calculated in self-consistent RPA using the exact finite-temperature Hartree solution as the basis function. For E_{10}, the energy difference between the first excited and the ground subbands of the unprimed ladder, our results are in reasonable agreement with finite-temperature infrared absorption measurements[13,14] over the whole temperature range. At low temperatures the many-body effects are of immense importance, whereas at higher temperatures they are still large but cancel out to a great extent for E_{10}, so that the Hartree approximation results apparently agree with the experiments also. This difference between low and high temperatures lies mainly in the exchange correction to subband 0 which diminishes considerably in magnitude from a large value at 0 K, as electrons are thermally excited out of the ground subband. Eventually, the self-energy corrections to both subbands 0 and 1 (which are then mainly due to correlation) become similar in magnitude, so that the effects drop out in the difference E_{10}. Most of the electrons thermally excited out of subband 0 occupy subband 0′ at higher temperatures, giving rise to a rather large exchange correction to $E_{0'}$. This is reflected in the fact that for the subband difference $E_{1'0'}$ the many-body corrections remain important also at high temperatures, as is observed in the experiment.[13,14] Quantitatively, however, the agreement between our theoretical results and the measured subband separations is decidedly worse for $E_{1'0'}$ than that for E_{10}. We have suggested two possible reasons for this: The position and occupancy of subband 0′ is uncertain because the interface potential barrier is not ideal, and many-body effects may not be described adequately within RPA because of the larger effective r_s of the electron gas in the primed subbands. To clarify this point we would like to see results of experimental measurements of $E_{1'0'}$ under such uniaxial stress that subband 0′ becomes the ground subband.

Another important element of this work has been the investigation of the extension to finite temperature of the LDF technique employed[3,18] earlier to calculate the electronic subband structure of the inversion layer at zero temperature. In this extension we neglect any explicit temperature dependence of the exchange-correlation potential, but retain its implicit temperature dependence through the electron density $n(z)$ which is calculated at finite temperature. We find that for the unprimed subbands this method works well in the whole temperature range 0—300 K, which allows us to conclude that for this subband ladder the implicit temperature effect is dominant. For the primed subbands, however, there is significant disagreement at elevated temperatures between the LDF and many-body perturbational results. This seems to indicate that for the primed subbands the explicit temperature becomes significant and again underscores that the primed subbands could be more interesting to study experimentally and theoretically without the complications coming from the unprimed subbands.

Our calculation of the single-particle energy spectrum in the space-charge layer involves a number of approximations, the influence of some of which is not easily estimated. We have used essentially RPA to calculate the self-energies. This approximation is exact in the high density ($r_s \to 0$) limit, but its actual validity in our case where $8 \geq r_s \geq 1.5$ for the unprimed subbands when

$10^{11} \leq N_s \leq 3 \times 10^{12}$ cm^{-2} is questionable. Nevertheless, for lack of manageable, demonstrably better approximations it is often used in metal physics in the same density regime.[25,33] The effect of dimensionality on the validity of RPA has also not been investigated systematically, although exchange-correlation effects are thought to be more important in two dimensions[34] compared with three for equivalent values of r_s. We do not expect serious errors relative to RPA from our use of the generalized plasmon-pole approximation for the screened interaction, since comparisons show only insignificant differences at $T=0$ in three[16] and two[2] dimensions and in the $T \to \infty$ limit.[5] Also, the diagonal approximation for the Coulomb interaction is well justified since off-diagonal elements are very small.

Finally, a possibly serious approximation is the neglect of the imaginary part of the self-energy both at zero and finite temperature. No satisfactory microscopic calculation of quasiparticle lifetimes in inversion layers exists. In the plasmon-pole approximation at $T=0$ the imaginary part of the self-energy is zero in the lowest subband below the Fermi level for most densities because it is difficult to fulfill momentum and energy conservation in the emission or absorption of a plasmon. For states in higher-lying subbands a scattering into the lowest subband by emission of a plasmon is quite possible and leads to a broadening of the state of several meV, much broader than the width of the experimentally measured resonance lines (~ 1 meV). Clearly this theory is insufficient to describe line shapes. The only reported theory by Nakamura *et al.*[6] also gives large values of the imaginary parts of the self-energy. Such large values would possibly give broad absorption lines whose maximum could conceivably be shifted appreciably.

The LDF technique in principle only works for the ground state of an inhomogeneous system and only if the density variations are slow compared with Fermi wavelengths.[19] It is, however, heavily used in systems where the density distribution by far violates the condition of slow variation, and empirically the method has had astounding success when its results are compared with experiments. Its successful application to the subband problem at $T=0$ (Refs. 3 and 8) is yet another empirical proof of its usefulness. Our extension to finite temperature must also be considered empirical, and we have shown in this paper that the method seems to work satisfactorily for the unprimed subbands, whereas the primed subbands might well provide a difficult test case for the method, also at low temperatures.

Finally, we must make some important remarks on the comparison of our theoretical calculation with experimental results. We have calculated single-particle energy levels of the system including electron-electron interaction effects. However, an intersubband spectroscopic experiment[9,12–14] measures the response of the multilevel system to the electric field of the infrared radiation. Thus resonant absorption takes place at the poles of the conductivity function, which in the long-wavelength limit is the same as the polarizability function of the interacting system.

For a noninteracting system the poles of the polarizability are at the energy differences E_{ji} of the single-particle levels, but as is known from optical properties of bulk semiconductors[35] the poles of the interacting system can be shifted due to the excitonic effect, i.e., vertex corrections. This shift is due to the interaction of the electron excited to a higher level and the hole left behind in the ground subband. This manifestly two-particle effect tends to lower the resonance pole corresponding to the $i \to j$ intersubband transition below the subband energy difference E_{ji}. In addition to the vertex corrections there is the so-called "depolarization shift" or "resonance screening" effect[36–38] which originates in the inhomogeneity of the system in the direction perpendicular to the interface. Because of this, the electron gas can screen the external radiation field even at long wavelengths, so that the total field inside the inversion layer is changed, and essentially the response to an external field has resonances where the response to an internal field has zeros, and not where it has poles. In many-body language this means that the reducible response function is quite different from the irreducible one.[2] This effect shifts the resonance up above the poles of the vertex corrected, irreducible response. Thus the two effects of vertex correction and depolarization shift tend to oppose each other.

The depolarization shift is a well defined quantity which can be calculated in a straightforward way. At $T=0$ it shifts the lowest resonance pole above E_{10} by as much as 15%. For the vertex corrections, approximations must necessarily be introduced, and there have been three different calculations of the excitonic effect. Ando[39] using a time-dependent LDF perturbational approach found that the vertex correction and the depolarization shift almost cancel each other, bringing the

resonance poles very close to the subband energy differences. On the other hand, Vinter[2,40] used the statically screened electron-hole interaction in the Bethe-Salpeter equation[30] and found a rather small effect. The most recent calculation was carried out by Das Sarma *et al.*,[41] who summed all the ladder bubble diagrams using a dynamically screened vertex and found results close to Ando's.[39] The latter authors were forced to make a number of other simplifying approximations owing to the complicated nature of the vertex corrections, and they concluded that it is hard to say anything definitive about the quantitative importance of those effects in the silicon inversion layer. For $T>0$ no calculation of the depolarization shift and vertex corrections exists, but a preliminary estimate[42] indicates that the relative importance of the two effects remains the same at finite temperature.

In addition to these problems of estimating with reasonable accuracy the interaction effects, we still have the problem mentioned in Sec. II for the quasiparticle energies: The subband energy differences are about 15% smaller when one solves Dyson's equation (10) than when one takes only the first iteration Eq. (11) at $T=0$.[2] Therefore, when one compares only with infrared absorption experiments both Vinter[2] and Ando[39] can claim excellent agreement even though they have different excitonic shifts, because their calculated subband separations differ by about 15%.

From the foregoing discussion we conclude that as long as experiments have not been made which measure directly subband energy differences, it is not possible to judge the merits of the various approximations. Theoretical efforts will hardly be able to decide these points, so at the moment we believe that 10% is a limit on the accuracy we can achieve in this complicated many-body system. Within this accuracy, we believe that our calculation, which for the first time has eliminated all the nonessential approximations of earlier finite-temperature work, is in quite satisfactory agreement with experiments in the whole temperature range 0–300 K. The present work brings our knowledge of the electronic structure of the silicon inversion layer at finite temperature to the same level of sophistication as that at zero temperature.

The system studied here is by far the most extensively studied space-charge layer, but the method outlined in this paper is applicable to space-charge layers in other systems with negligible nonparabolicity. We intend to apply it to other experimentally interesting systems like Si(110)- and Si(111)-SiO_2 (Ref. 43) and the InP inversion layer.[44,45]

ACKNOWLEDGMENTS

The authors are grateful to F. Schäffler for useful discussions on experimental results. This work was supported in part by the National Science Foundation through Grant No. DMR 7908819 and Deutsche Forschungsgemeinschaft via SFB 128.

*Present address.
[1]F. Stern, Phys. Rev. B 5, 4891 (1972).
[2](a) B. Vinter, Phys. Rev. B 13, 4447 (1976); (b) 15, 3947 (1977).
[3]T. Ando, Phys. Rev. B 13, 3468 (1976).
[4]F. J. Ohkawa, Surf. Sci. 58, 326 (1976); Ph. D. thesis, University of Tokyo, 1975 (unpublished).
[5]S. Das Sarma, R. K. Kalia, M. Nakayama, and J. J. Quinn, Phys. Rev. B 19, 6397 (1979); R. K. Kalia, S. Das Sarma, M. Nakayama, and J. J. Quinn, *ibid.* 18, 5564 (1978).
[6]K. Nakamura, H. Ezawa, and K. Watanabe, Phys. Rev. B 22, 1892 (1980).
[7]S. Das Sarma and B. Vinter, Phys. Rev. B 23, 6832 (1981).
[8]T. Ando, Surf. Sci. 73, 1 (1978).
[9]P. Kneschaurek, A. Kamgar, and J. F. Koch, Phys. Rev. B 14, 1610 (1976).
[10]R. G. Wheeler and H. S. Goldberg, IEEE Trans. Electron Devices ED-22, 1001 (1975).
[11]D. C. Tsui and G. Kaminsky, Phys. Rev. Lett. 35, 1468 (1975).
[12]P. Kneschaurek and J. F. Koch, Phys. Rev. B 16, 1590 (1977).
[13]F. Schäffler and F. Koch, Solid State Commun. 37, 365 (1981).
[14]F. Schäffler, Diplom thesis, Technical University of Munich, 1980 (unpublished).
[15]A. L. Fetter and J. D. Walecka, *Quantum Theory of Many-Particle Systems* (McGraw-Hill, New York, 1971).
[16]B. I. Lundqvist, Phys. Kondens. Mater. 6, 193 (1967); 6, 206 (1967); 7, 117 (1968).
[17]A. W. Overhauser, Phys. Rev. B 3, 1888 (1971).
[18]B. Vinter, Solid State Commun. 32, 651 (1979).
[19]W. Kohn and L. J. Sham, Phys. Rev. 140, A 1133 (1965); L. J. Sham and W. Kohn *ibid.* 145, 561 (1966).
[20]For a system without interactions via the image, U. Gupta and A. K. Rajagopal, Phys. Rev. A 22, 2792

(1980) have calculated a temperature-dependent exchange-correlation potential.
[21]T. M. Rice, in *Solid State Physics,* edited by F. Seitz, D. Turnbull, and H. Ehrenreich (Academic, New York, 1978); Vol. 32, p. 1.
[22]D. A. Liberman, Phys. Rev. B 20, 4981 (1979).
[23]W. L. Bloss, L. J. Sham, and B. Vinter, Phys. Rev. Lett. 43, 1529 (1979); Surf. Sci. 98, 250 (1980).
[24]D. F. Dubois, Ann. Phys. (N.Y.) 7, 174 (1959); 8, 24 (1959).
[25]T. M. Rice, Ann. Phys. (N.Y.) 31, 100 (1965).
[26]S. Das Sarma, Ph.D. thesis, Brown University, 1979 (unpublished).
[27]U. von Barth and L. Hedin, J. Phys. C 5, 1629 (1972); O. Gunnarsson and B. I. Lundqvist, Phys. Rev. B 13, 4274 (1976).
[28]F. Stern, Solid State Commun. 21, 163 (1977).
[29]M. Nakayama, Surf. Sci. 98, 358 (1980).
[30]D. Pines and P. Nozières, *The Theory of Quantum Liquids* (Benjamin, New York, 1966).
[31]P. Stallhofer, J. P. Kotthaus, and G. Abstreiter, Solid State Commun. 32, 655 (1979).
[32]F. Stern and W. E. Howard, Phys. Rev. 163, 816 (1967).
[33]L. Hedin and S. Lundqvist, in *Solid State Physics,* edited by F. Seitz, D. Turnbull, and H. Ehrenreich (Academic, New York 1969), Vol. 23, p. 1.
[34]M. Jonson, J. Phys. C 9, 3055 (1976).
[35]W. Hanke and L. J. Sham, Phys. Rev. Lett. 43, 387 (1979); Phys. Rev. B 12, 4501 (1975).
[36]W. P. Chen, Y. J. Chen, and E. Burstein, Surf. Sci. 58, 263 (1976).
[37]S. J. Allen, Jr., D. C. Tsui, and B. Vinter, Solid State Commun. 20, 425 (1976).
[38]M. Nakayama, Solid State Commun. 21, 587 (1977).
[39]T. Ando, Z. Phys. B 26, 263 (1977).
[40]B. Vinter and F. Stern, Surf. Sci. 58, 141 (1976).
[41]S. Das Sarma, R. K. Kalia, M. Nakayama, and J. J. Quinn, Phys. Rev. B 24, 7181 (1981).
[42]S. Das Sarma (unpublished).
[43]T. Cole and B. D. McCombe, J. Phys. Soc. Jpn. 49, Suppl. A 959 (1980).
[44]K. von Klitzing, Th. Englert, and D. Fritzsche, J. Appl. Phys. 51, 5893 (1980).
[45]H. C. Cheng and F. Koch, Solid State Commun. 37, 911 (1981).